

This is the accepted manuscript version of the contribution published as:

Hegner, R., Rosa, L.F.M., Harnisch, F. (2018):

Electrochemical CO₂ reduction to formate at indium electrodes with high efficiency and selectivity in pH neutral electrolytes

Appl. Catal. B-Environ. **238**, 546 – 556

The publisher's version is available at:

<http://dx.doi.org/10.1016/j.apcatb.2018.07.030>

Electrochemical CO₂ reduction to formate at indium electrodes with high efficiency and selectivity in pH neutral electrolytes

Richard Hegner, Luis F. M. Rosa and Falk Harnisch*

Helmholtz Center for Environmental Research GmbH - UFZ,
Department of Environmental Microbiology,
Permoserstraße 15 / 04318 Leipzig / Germany

*Correspondence to:

PD Dr. Falk Harnisch (falk.harnisch@ufz.de)

Abstract

Electrochemical reduction of CO₂ is promising for a bio-based economy as it combines utilization of CO₂ as feedstock and provides a pathway for the utilization and (temporary) storage of electric energy. Among different products formate (HCOO⁻) can be produced with high rates and selectivity using indium as electrocatalyst. This can be achieved at mild biocompatible reaction conditions, e.g. ambient temperature, ambient pressure and neutral pH. Formate can serve as a source of carbon and energy for the biosynthesis of energy carriers or chemicals. However, the *in situ* interfacing of electrochemical CO₂ reduction and biosynthesis creates challenges for electrochemical engineering. It is demonstrated that the electrode potential is the main steering parameter affecting the coulombic efficiency, selectivity and rate of formate production in NaHCO₃ electrolyte solution at biocompatible conditions. Coulombic efficiencies and formate production rates of $94.5 \pm 2\%$ and $0.136 \pm 0.016 \text{ mmol h}^{-1} \text{ cm}^{-2}$ (at -2.2 vs. Ag/AgCl and $\kappa = 10 \text{ mS cm}^{-1}$), respectively, were achieved. Further, increasing the conductivity using inert electrolytes can enhance formate space-time yields up to $0.254 \pm 0.031 \text{ mmol h}^{-1} \text{ cm}^{-2}$. Surprisingly, high NaHCO₃ concentrations do not further increase formate production which supports that HCO₃⁻ is not electrochemically converted but only acting as CO₂ / H⁺ reservoir. Based on kinetic modeling insight on the inter-conversion of the carbonaceous species by CO₂ sparging of the electrolyte solution is provided. Importantly, the influence of O₂ on the electrochemical CO₂ reduction was revealed to be marginal. This study, providing principles on the engineering of electrochemical CO₂ reduction to formate for future interfacing to biosynthesis, demonstrates its feasibility to become technologically relevant.

Key words

electrobiotechnology, electrobiorefinery, electrocatalysis, carbon dioxide reduction

1 Introduction

The concentration of the greenhouse gas CO₂ in the atmosphere is continuously rising. This is due to growing population, intensified agriculture, increased deforestation and land use as well as growing industry and the associated exploitation of fossil resources [1-3]. In 2015 on the global scale 31 % of the total CO₂ emission originated from coal-fired power plants [4]. Sustainable economy therefore calls for technologies using CO₂ as feedstock for chemicals and fuels. Consequently, a promising concept is the electrochemical reduction of CO₂ that combines two advantages. First, using CO₂ as feedstock and second, providing a pathway for the utilization and (temporary) storage of electric energy [5, 6]. Depending on the applied conditions and electrode materials used different products can be gained including for instance CO, CH₄ and formic acid (HCOOH), as well also short-chain hydrocarbons like ethylene [7, 8]. Among the obtained products formic acid – being present as formate (HCOO⁻) at neutral pH – is, despite its low energetic value, an attractive product due to its (bio)chemical versatility [9].



$$E_{CO_2}^0 = -0.430 \text{ V vs. SHE at pH 7 and } 25 \text{ }^\circ\text{C}$$

For instance it is used as chemical building block in the pharmaceutical industry [10], as feedstock for animal fodder preservation, in textile industry [11], and as fuel for fuel cells [12]. Further, it serves as (temporary) storage molecule for H₂ gained from renewably produced electric energy [13-16]. The reduction of CO₂ to formate (Eq. (1)) can be achieved at mild reaction conditions, e.g. ambient temperature, ambient pressure and neutral pH, and thereby fulfilling several criteria of green chemistry [17, 18].

However, formate is highly soluble in aqueous solutions and hence requires an energy- and therefore also cost-intensive product extraction. Interestingly, formate can also serve as substrate, i.e. carbon, energy and electron source, for the microbial biosynthesis of energy carriers or fine and bulk chemicals [10, 19, 20]. Therefore, when performing electrochemical CO₂ reduction *in situ* – meaning in the biological process media – extraction of formate is not needed.

All endeavors for the interfacing of microbial and electrochemical conversions for bio-production can be summarized under the umbrella of the electrobiorefineries [21]. Electrobiorefineries allow the coupling of electrochemical and microbial conversions for the storage and exploitation of electric energy. In addition to approaches based on the immediate transfer of electrons between electrodes and microorganisms in primary microbial electrochemical technologies (MET) [22] the more indirect utilization of electrochemical reactions in secondary MET and hybrid systems are increasingly considered. It was recently shown that bio-based chemicals, e.g. drop-in fuels [23], polyamides [24] or higher alcohols [1], can be gained from the electrochemical upgrading of microbial metabolites. Within electrobiorefineries also the electrochemical reduction of CO₂ to formate can play a key role. This was first demonstrated by Li and co-workers [20]. In their study electrochemical CO₂ reduction to formate was coupled to its microbial conversion to higher alcohols by an engineered *Cupriavidus necator* strain in the same process medium. The here followed concept of electrochemical CO₂ reduction to formate *in situ* creates challenges for electrochemical engineering. Most important is the need to design an efficient and robust electrochemical process at biocompatible conditions characterized by near neutral pH, ambient temperature and pressure as well as physiologic salinity and the presence of components of microbial media like amino acids, vitamins and trace metals [17].

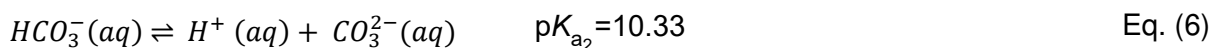
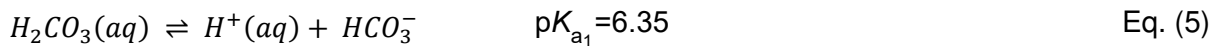
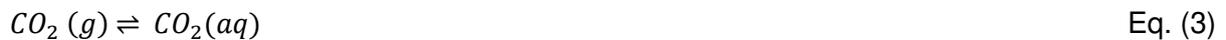
An electrocatalyst with high selectivity for formate production from CO₂ in aqueous solution is indium (In). This can be attributed to its high overpotential for the hydrogen evolution reaction (HER, Eq. (2), see SI section *SI 1.2* for overpotentials) [25].



$$E_{H_2}^0 = -0.414 \text{ V vs. SHE at pH 7 and } 25 \text{ }^\circ\text{C}$$

Uncovering the mechanism of electrochemical CO₂ reduction to formate on metals like In or more frequently Sn was research focus of many studies in the past years and has been recently reviewed by Lee *et al.* [26]. The debate on the reaction mechanism, i.e. formed intermediates of electrochemical CO₂ reduction, is still ongoing since electrokinetic studies and spectroscopic techniques like IR and Raman analysis partially propose different mechanisms. This hinders the straightforward engineering of the electrode material and therefore also of the overall process [17].

Effects of sparging CO₂(g) into an electrolyte solution have been rarely studied [27]. As described by Eq. (3) to Eq. (6), gaseous CO₂ dissolves in the electrolyte solution and reacts with H₂O to H₂CO₃ that further equilibrates to HCO₃⁻ and CO₃²⁻ and protons [28-30].



Sparging of the electrolyte solution with CO₂(g) influences the pH [27] and, as can be seen by Eq. (3) to Eq. (6), also affects the chemical equilibria and hence the availability of the potential reactant of the electrochemical CO₂ reduction.

Based on a robust and highly reproducible experimental system [17] we systematically investigate and highlight the importance of operational parameters, including the applied potential, E_{WE} , electrolyte solution conductivity, κ , carbonate concentration, pH, and oxygen for the electrochemical CO₂ reduction in pH neutral electrolyte solutions. Based on kinetic modeling insights on the inter-conversion of the carbonaceous species by CO₂ sparging of

the electrolyte solution is provided. Finally, implications for the *in situ* coupling of electrochemical CO₂ reduction and bio-production are addressed.

2 Material and Methods

If not stated otherwise all experimental potentials refer to Ag/AgCl (saturated KCl, 0.197 V vs. standard hydrogen electrode (SHE)). For thermodynamic calculations experimental potentials are re-calculated and provided *versus* SHE as detailed in the formulas.

2.1 Chemicals

All chemicals were of at least analytical grade. All solutions were prepared with de-ionized water (Merck Millipore, USA). Sodium acetate, NaHCO₃ and HCl (37 %) were obtained from Carl Roth GmbH (Germany), H₂SO₄ was supplied by Merck KGaA (Germany) and Na₂SO₄ (anhydrous, > 98%) by CHEMSOLUTE® Th. Geyer GmbH (Germany). The In salt InCl₃ (anhydrous, 99.999%) was obtained from Chempur (Germany). CO₂ (99.5 mol-% purity), carrier gases (99.999 mol-% purity) and calibration gases for gas chromatography were purchased from Air Products GmbH (Germany). Compressed air (CA) was used as an air-like gas mixture with 78 Vol-% N₂ and 21 Vol-% O₂.

2.2 Experimental setup

Electrochemical pre-treatment, the deposition of the electrocatalyst as well as the electrochemical CO₂ reduction were performed in a 300 mL-glass vessel equipped with a tailor-made lid as described previously [17] and shown in Figure 1. The lid was printed from poly lactic acid (Innofil3D, The Netherlands) using a 3D printer (Ultimaker 2+, Ultimaker, The Netherlands) containing ports for each electrode, sampling, and gassing. For electrochemical CO₂ reduction in the gas tight system (see below) the setup was slightly modified by adding an additional exhaust gas port, using rubber sealing and further insulating the inner lid by

coating with HT-2 Epoxy glue (R&G Faserverbundwerkstoffe GmbH, Germany) and silicon (RECA NORM GmbH, Germany) to assure gas tightness of the system while keeping the geometric dimensions. All experiments were carried out under potentiostatic control by a potentiostat/galvanostat (SP-200, BioLogic Science Instruments, France) using a three-electrode setup consisting of a working electrode (WE), an Ag/AgCl reference electrode (RE, SE 11, 0.197 V vs. SHE Sensortechnik Meinsberg, Germany) and a counter electrode (Platinode, 0.05 x 1 x 7 cm, Umicore Galvanotechnik GmbH, Germany). The working electrode backbone and current collector was a graphite rod of high purity (99.997 %, Ø 0.635 x 6 cm, particle size of 21 to 100 µm, Goodfellow, UK). The graphite backbone was connected *via* a custom-made adapter made from acrylic glass (PMMA) fixed to a rotating electrode holder/contacter (CTV 101T, Tacussel, France). The system was always operated as a two-chamber electrochemical cell except for the In deposition. The counter electrode was separated *via* a custom-made glass tube interfaced *via* an ion exchange membrane (fumasep FKE, FuMA-Tech GmbH, Germany). A micro-filter-candle made from glass (pore size 16-40 µm, Ø 9 mm, ROBU Glasfilter-Geräte GmbH, Germany) served as gas sparger which was immersed in the electrolyte solution facing the WE. For electrochemical pre-treatment and deposition of the catalyst the electrolyte solutions were purged with nitrogen at a flow rate of 0.08 L min⁻¹ (20 °C, 1 bar). If not stated otherwise, throughout the electrochemical CO₂ reduction experiments the electrolyte was purged with CO₂ at a flow rate of 0.06 L min⁻¹ (20 °C, 1 bar) set by a rotameter (ABB Fisher & Porter, Germany). For all connections gas tight Tygon® tubes (Fisher Scientific, USA) were used. In experiments with the requirement of continuously exchanging the anolyte, it was pumped with a peristaltic pump (ISMATEC Reglo Analog MS-4/8, Cole-Parmer GmbH, Germany) from a 500 mL reservoir to the counter electrode chamber and from there to a 500 mL waste tank with a flow rate in the range of 0.6 mL min⁻¹ to 2 mL min⁻¹. All experiments were conducted at 30 °C in a climate chamber and the medium was mixed *via* a magnetic stir bar at a specific rotation rate.

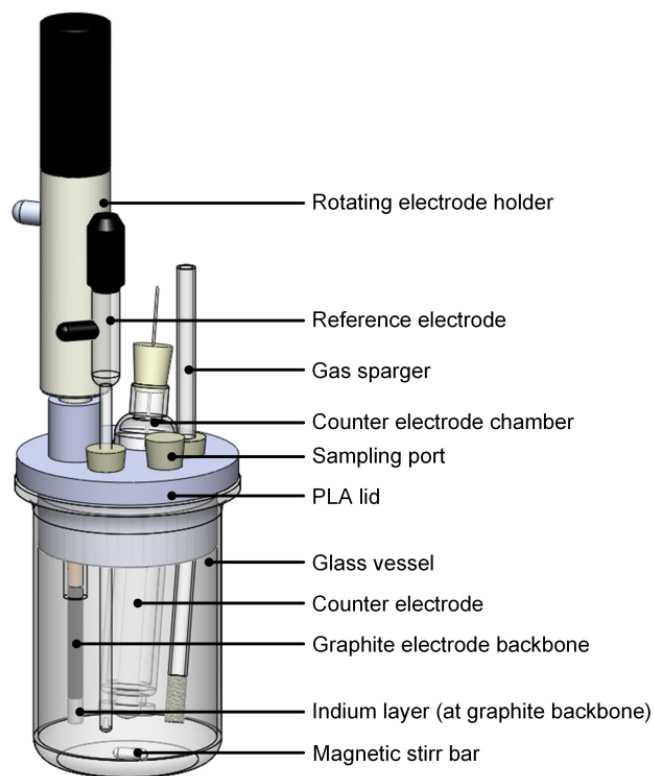


Figure 1: Scheme of the tailor-made electrochemical cell for pretreatment, In deposition and electrochemical CO₂ reduction to formate (details see section 2.2).

2.3 Electrode preparation

2.3.1 Graphite backbone pre-treatment

The mechanical and electrochemical pre-treatment of the graphite electrode backbone was conducted as described previously by Gimkiewicz *et al.* [17].

2.3.2 Electrodeposition of Indium on the graphite electrode backbone

As described by Gimkiewicz *et al.* [17], linear sweep voltammetry was performed from $E_i = 0$ V to $E_{\text{depos}} = -0.9$ V in 50 mL of 0.1 M InCl₃ in 1 M de-aerated acetate buffer (pH 4.5, N₂ purging at a flow rate of 0.08 L min⁻¹ at least 10 min prior to the start of the electrodeposition procedure) at a scan rate of $\nu = 20$ mV s⁻¹. E_{depos} was held until a defined charge (Q_{depos}) of 0.68 C per cm² surface area (C cm⁻²_{geometric}, corresponding to a total charge of 1.7 C for an

electrode surface area of 2.51 cm²) was reached and the WE was rotated at 10 rpm during the whole electrodeposition procedure. The specific charge for In loading on the graphite backbone corresponds to 1975 atomic layers of In in average and a total amount of 0.635 mg In for an electrode surface of 2.51 cm². Before further use the electrode was washed with de-ionized water. The acetate buffer containing the In salt was kept for recycling and reuse (see section 2.3.3).

2.3.3 Indium catalyst recycling

Unless stated otherwise In was recovered from the graphite electrode backbone by potential-sweep stripping In³⁺ back into de-aerated In deposition solution (see section 2.3.2) as described by Gimkiewicz *et al.* [17]. Parameters set for the CV were $E_i = -0.9$ V, $E_1 = 1$ V, and $E_2 = 0$ V at a scan rate of $v = 20$ mV s⁻¹ and de-aeration was performed by continuous N₂ purging of the In deposition solution for at least 5 min prior to the start of the procedure.

2.4 Electrochemical CO₂ reduction to formate

Table 1: Compilation of different electrolyte solutions used in this study and their respective properties.

C_{NaHCO_3} [M]	conductivity adjusted with Na ₂ SO ₄	conductivity ($T = 298 \text{ K}$) [mS cm ⁻¹]	C_{Na^+} [mM]	pH ^a _{pre CO₂} [-]	pH _{Start} [-]	pH _{End} [-]
0.01	yes	37	10	8.6	5.8	6.5
	no	4.5	50			
0.05	yes	10	124	8.8	6.5	6.6
	yes	20	293			
	yes	37	580			
0.5	no	37	500	9.4	7.3	7.4
	yes	37	n.a.	9.4	7.3	7.4

^a this parameter describes the pH of the respective NaHCO₃ solution before the CO₂ purging of the NaHCO₃ solutions for a period of 10 minutes prior to start of the experiment (see section 2.4.1)

2.4.1 Standard procedure

After the In deposition the electrode was placed in 50 mL electrolyte solution of different NaHCO₃ concentration and/or adjusted conductivity as listed in Table 1. The duration of all experiments was 1 h and in order to avoid acidification of the anolyte, it was continuously pumped through the counter electrode chamber from an anolyte reservoir with a flow rate ranging from 0.6 mL min⁻¹ to 2 mL min⁻¹ (see section 2.2). Prior to CO₂ sparging into the electrolyte solution in the WE chamber the electrolyte solutions in both chambers were identical. The conductivity of the electrolyte solution was measured with a conductivity meter (SevenExcellence S470, Mettler-Toledo, Germany) and pH was measured with a drop pH meter (LAQUAtwin B-712, Japan). Both parameters were determined for the electrolyte solution with and without CO₂ purging prior to the start of the experiment. After at least 10 min of CO₂ purging of the electrolyte solution the experiments were started.

2.4.1 Addition of supporting electrolyte

In order to adjust the conductivity of the electrolyte solution Na₂SO₄ as supporting electrolyte was added (see Table 1).

2.4.2 Purging with different ratios of CO₂/air

The adjustment of the ratio of CO₂ and CA was conducted by keeping the CO₂ flow rate stable at 0.06 L min⁻¹ while adjusting the flow rate of CA in a range between 0 L min⁻¹ and 0.06 L min⁻¹. Both gas streams were mixed by joining the gas flows in one tube using a Y-hose connector. For channeling the gases, gas tight Tygon® tubes (Fisher Scientific, USA) were used and the gas flow rates of the gases were controlled by precision rotameters (FI-585 for CO₂ and FI-464 for air) of a Biostat B-DCU II bioreactor system (Sartorius, Germany).

2.5 Liquid phase analysis

2.5.1 HPLC analysis

HPLC (Shimadzu Scientific Instruments, USA) measurements of the aqueous liquid phase were performed with a photodiode array detector (SPD-M20A prominence, Shimadzu Scientific Instruments, Japan) using a Hi-Plex H column (300 mm x 7.7 mm ID, 8 µm pore size, Agilent Technologies, Germany) equipped with a pre-column (Carbo-H 4 mm x 3 mm ID, Security Guard, Phenomenex). Isocratic elution at 50 °C with 5 mM H₂SO₄ was set at 0.5 mL min⁻¹ for 30 min⁻¹. Peak identification and calibration of formate was carried out with external standards (0.1 mM to 22.2 mM, six- point calibration; calibration limit is 0.1 mM, $R^2=0.99$). The samples were analyzed immediately after sampling and formate was the only produced analyte which was detected in the liquid phase. For long-term storage the liquid samples were stored at -20 °C.

2.5.2 Indium determination within the electrolyte solution

For determining the In loss to the electrolyte solution ICP-MS measurements of the liquid phase were performed using ELEMENT™ XR sector field ICP-MS (Thermo Fisher Scientific, Germany) in technical triplicates. Integration time for In was set to 2 seconds at a m/z of 115 and a mass resolution of 300. Calibration was conducted with external In standards (0 µg L⁻¹

to $2 \mu\text{g L}^{-1}$, six-point-calibration, $R^2 = 0.99$). ^{103}Rh was added as internal standard to the diluted sample solution at a concentration of $1 \mu\text{g L}^{-1}$ to correct for signal drifts.

2.6 Gas phase analysis

For measuring the headspace gas composition during electrochemical CO_2 reduction the standard setup (see section 2.2 and Figure 1) was slightly modified to a gas tight system. A complete flow scheme of the experimental setup allowing the determination of a closed gas balance is depicted in Figure S1. The volume of the off-gas was measured by a mass flow meter which was connected to a gas chromatograph equipped with a thermal conductivity detector (GC-TCD). The headspace of the electrochemical cell was sampled every 10 minutes. For all connecting tubes gas tight Tygon® tubes (Fisher Scientific, Pittsburgh, USA) were used. For further details see SI section *SI 1.1*.

2.7 Data processing and calculations

2.7.1 Coulombic efficiencies (CE) and production rates (r)

The Coulombic efficiency (CE) for electrochemical formate production was calculated by setting the charge transferred to formate (Q), derived from the actual produced mass m of formate within the electrolyte solution (volume of the electrolyte solution was assumed to be constant over time) determined by HPLC analysis, in relation to the total charge (Q_{total}):

$$CE = \frac{Q}{Q_{total}} \times 100\% \quad \text{Eq. (7)}$$

with

$$Q = \frac{m}{M} zF \quad \text{Eq. (8)}$$

where $M = 45 \text{ g mol}^{-1}$ is the molar mass of formate, $z = 2$ is the number of transferred electrons per CO_2 molecule, and $F = 96485 \text{ C mol}^{-1}$ is the Faraday constant. Q_{total} can be derived from the integrated current (i) of the electrochemical CO_2 reduction:

$$Q_{total}(t) = \int_0^t i(t) dt \quad \text{Eq. (9)}$$

The formate production is given as rate (r in $\text{mmol h}^{-1} \text{ cm}^{-2}$) and was normalized to the geometric working electrode surface area ($A_{WE_{geom}}$ in cm^2).

$$r = \frac{\Delta m}{M \times A_{WE_{geom}} \times \Delta t} \quad \text{Eq. (10)}$$

The Coulombic efficiency for electrochemical H_2 production CE_{H_2} is expressed as the mean of a function over time ($\overline{CE}_{\text{H}_2}(t)$) and was calculated by relating the charge transferred to H_2 ($Q_{\text{H}_2}(t)$), derived from the actual produced moles $n_{\text{H}_2}(t)$ of H_2 determined by GC-TCD and gas mass flow analysis, in relation to the charge produced in the time period until time point t ($Q_{total}(t)$):

$$CE_{\text{H}_2}(t) = \frac{\int_0^t \overline{CE}_{\text{H}_2}(t) dt}{\Delta t} \quad \text{Eq. (11)}$$

with

$$\overline{CE}_{\text{H}_2}(t) = \frac{Q_{\text{H}_2}(t)}{Q_{total}(t)} \times 100\% \quad \text{Eq. (12)}$$

with

$$Q_{\text{H}_2}(t) = n_{\text{H}_2}(t) \times z \times F \quad \text{Eq. (13)}$$

n_{H_2} is the number of H₂ molecules in moles, $z = 2$ the number of electrons per H₂ molecule and $F = 96485 \text{ C mol}^{-1}$ is the Faraday constant. n_{H_2} was calculated as follows:

$$n_{H_2}(t) = \frac{p_{H_2}(t)}{100} \times V_m \times N_A \times CF \times \int_0^t V(t) \quad \text{Eq. (14)}$$

where p_{H_2} is the proportion of H₂ in mol-% detected in the off-gas, $V(t)$ is the measured off-gas volume until time point t in mL, V_m is the molar volume of ideal gases ($T = 303.15 \text{ K}$, 1 atm) of 24.88 L mol^{-1} , N_A is the Avogadro constant in mol^{-1} , and CF is a dimensionless gas conversion factor for the specific gas composition measured, calculated by the calculation routines of the FLUIDAT® on the Web software (V1.56, Bronkhorst High-Tech B.V., The Netherlands).

The hydrogen production rate ($\bar{r}_{H_2}(t)$ in $\text{mmol h}^{-1} \text{ cm}^{-2}$) is expressed as the mean of a function of time and was normalized the geometric working electrode surface area ($A_{WE_{geom}}$ in cm^2).

$$r_{H_2}(t) = \frac{\int_0^t \bar{r}_{H_2,n}(t) dt}{\Delta t} \quad \text{Eq. (15)}$$

with

$$\bar{r}_{H_2}(t) = \frac{n_{H_2}(t)}{A_{WE_{geom}} \times \Delta t} \quad \text{Eq. (16)}$$

The total Coulombic efficiency CE_{total} of all products is calculated as the sum of the single coulombic efficiencies of all products detected in the liquid phase (formate) and the gaseous phase (H₂).

$$CE_{total} = CE + CE_{H_2} \quad \text{Eq. (17)}$$

2.7.2 Power input

The electrical power input for the production of 1 mol formate, $P_{formate}$, is the power P_{total} for the electrochemical half cell of the WE integrated over time and normalized by the amount of formate produced ($n_{formate}$) from electrochemical CO₂ reduction as determined by HPLC analysis. E_{WE} used for calculating P_{total} was referred to a Ag/AgCl reference electrode:

$$P_{formate} = \frac{P_{total}}{n_{formate}} \quad \text{Eq. (18)}$$

with

$$P_{total}(t) = -E_{WE} (vs. Ag/AgCl) \times \int_0^t i(t) dt \quad \text{Eq. (19)}$$

2.7.3 Selectivity for formate production

The selectivity, S , for formate production is defined as ratio of the gained products as follows:

$$S = \frac{n_{formate}}{n_{H_2}} \quad \text{Eq. (20)}$$

where $n_{formate}$ is derived from HPLC measurements and n_{H_2} is considered as the only side product. This assumption is based on the confirmation of a closed e⁻-balance (see section 3.1).

2.7.4 Statistical analysis

For characterizing significant effects ANOVA was performed using a *student's t*-test of the respective results (*OriginPro* software (OriginLab, Northampton, USA)). In case of unequal sample numbers the *Welch's t*-test (unequal variance *t*-test) was applied for the calculation of the *p*-value. The confidence interval for both *t*-tests was 95 %.

As stated in the text and captions, all experiments were conducted with minimum number of at least three independent replicates ($n = 3$) or more. In this regard independent replicates mean that the procedure of In deposition, subsequent formate production, and finally In

stripping was performed for each single replicate. All values are provided as the mean \pm confidence interval (CI , $\alpha = 0.05$).

2.8 Modeling of the aqueous CO_2 to $\text{HCO}_3^-/\text{CO}_3^{2-}$ inter-conversion and the gassing of CO_2 into the aqueous system

A model for simulation of CO_2 sparging into the aqueous system and the aqueous CO_2 to $\text{HCO}_3^-/\text{CO}_3^{2-}$ inter-conversion was implemented in COMSOL Multiphysics® using the chemical reactions as described in Schulz *et al.* [31]. Furthermore, the rate constants and approximations to salt-water and brackish water conditions were implemented as described in Schulz *et al.* [31] and Stumm and Morgan [32], respectively (for detailed information see the SI section *SI 1.3*).

3 Results and discussion

3.1 Potential dependence of the electrochemical CO₂ reduction to formate

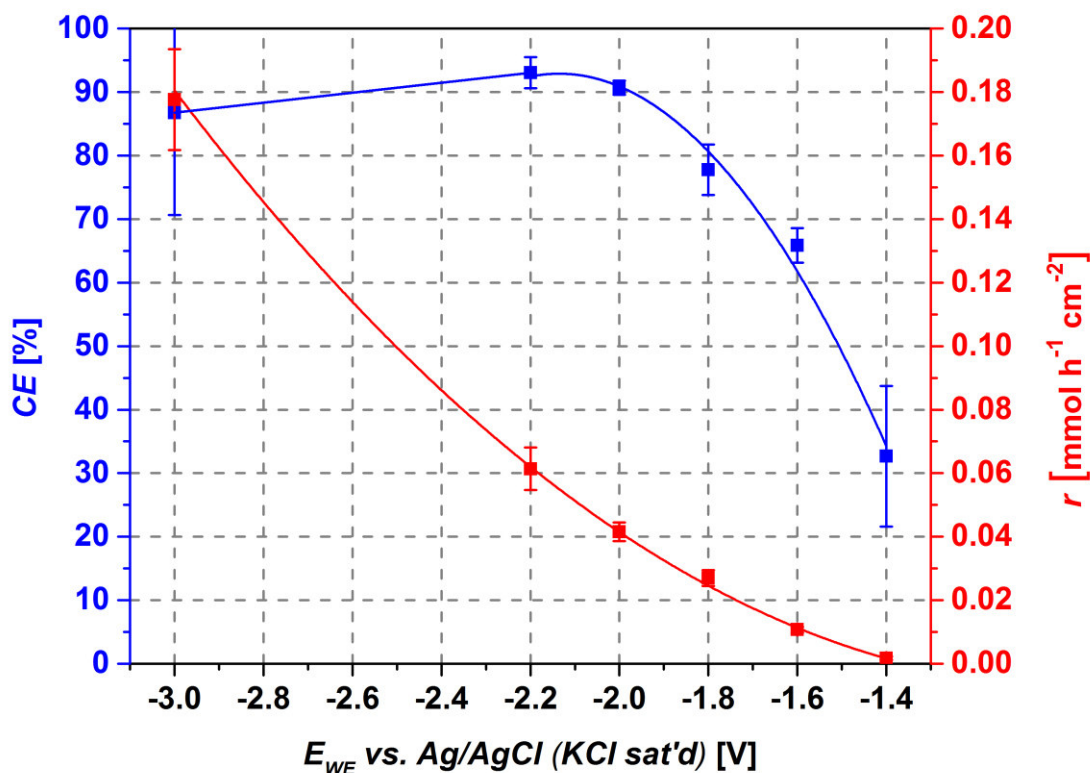


Figure 2: Potential dependence of the electrochemical CO₂ reduction to formate at In electrodes. Blue: coulombic efficiency (CE) and red: rate (r) of electrochemical CO₂ reduction to formate. All experiments were conducted in 0.05 mol L⁻¹ NaHCO₃ (pH 6.5) as electrolyte solution with $\kappa = 4.5$ mS cm⁻¹; $n = 6$ except for $E_{WE} = -3.0$ V $n = 3$. Reported values are mean values and the error bars represent the confidence interval ($\alpha = 0.05$).

The electrochemical CO₂ reduction strongly depends on the applied working electrode potential, E_{WE} , as for instance exemplarily shown previously for Cu, Sn as well as for In [2, 7, 33-36]. However, systematic studies on the effect of key process parameters including E_{WE} for the electrochemical CO₂ reduction on In electrodes are scarce.

As shown in Figure 2 when using electrodeposited In on a graphite backbone as electrocatalyst a strong increase for both parameters, CE and rate of formate production, r ,

from CO₂, for more negative E_{WE} can be revealed. Formate was the only product detected in the liquid phase. The CE shows saturation behavior for potentials more negative than -2.0 V (vs. Ag/AgCl, as all experimental potentials provided in this article) with a maximum CE of $93.0 \pm 2.4 \%$ for a 1 h formate production at a E_{WE} of -2.2 V. The rate increases exponentially for more negative potentials with the highest r reached at the studied most negative potential of $E_{WE} = -3.0$ V, still possessing a high CE of $86.8 \pm 16.1 \%$. The number of studies using more negative E_{WE} than -2.0 V is low. Noteworthy, the here reported CE is the highest reported for such negative E_{WE} . For instance Kaneco *et al.* [37] reported a CE of $\approx 70 \%$ when applying -3.0 V for formate production using an In wire of 99.99 % purity.

The increase of CE and r highlight that the E_{WE} is a crucial process parameter in order to drive and control the electrochemical reduction of CO₂ to formate. Further, it shows that applying more negative E_{WE} does not only increase the rate of formate production, even more surprising it shifts the selectivity of the reaction towards formate as indicated by the increase of the CE and discussed in section 3.4. Noteworthy, H₂ from the HER is the only side product as proven by GC measurements of experiments conducted in the gas tight experimental set-up (see SI section *SI 1.1* and Figure S1).

The overpotentials (see Eq. (SI 1) and (SI 3)) of the formate production, $\eta_{CO_2/HCOO^-}$, and of the HER, η_{2H^+/H_2} , calculated for the conditions applied ($E_{WE} = -2.2$ V; $T = 303$ K; pH 6.5, CO₂ saturated electrolyte solution (33 mM), $a_{HCOO^-} = 3.65$ mM (final concentration after a 1 h production process)) are 1.725 V and 1.703 V, respectively (see Table S2 and Table S3). As both overpotentials are in a narrow potential range, this suggests that the observed behavior is very likely to be caused by mechanistic or kinetic but not by thermodynamic effects. An increase of the CE with decreasing E_{WE} was already observed for anodized In electrodes [34]. The anodization pre-treatment of the In electrodes leads to the formation of an In-oxide layer. In their study Detweiler *et al.* [34] argue that an In-OH layer formed at the electrode surface by an acid-base reaction of the In-oxide layer with electrolyte solution suppresses the

HER at more negative potentials. Furthermore, it was observed that also the CE for the formation of CO, a known side product or intermediate for In and Sn based electrodes, drops with more negative E_{WE} [34]. This behavior was independent from In electrode pretreatment and therefore also independent from the oxidation state of the catalyst. Surprisingly, in this study no CO was detected over the whole range of E_{WE} tested. However, it has to be stressed that the e^- -balance, i.e. the CE_{total} (see Eq. (17)) of all detected products, for all experiments was closed and only for a E_{WE} of -1.6 V the e^- -balance could not be fully closed, leaving roughly 7 % of unbalanced e^- (see Figure S2).

According to Hori *et al.* [38] and others investigating Hg [39-42], bimetallic Ag-Sn [5] or pure Sn and In [43] as electrocatalyst, another explanation for the strong potential dependency is the limitation by the first reaction step being a one-electron-transfer to CO_2 to form $^{\cdot}CO_2^-$ as intermediate species. This reaction was identified as the rate limiting step by electrokinetic studies as the formation of this intermediate requires higher overpotentials than the subsequent reactions to finally yield formate (at Hg electrodes) [39, 42].

The results presented in Figure 2 are in line with indications reported in literature, however, here proven with sufficient statistical certainty. Although mechanistic conclusions cannot be drawn, it becomes clear that the electrochemical CO_2 reduction to formate is not thermodynamically limited, revealing its engineering potential.

Based on the high reproducibility of the used set-up and workflow, effects of further key process parameters, i.e. the electrolyte conductivity and the $NaHCO_3$ concentration, were systematically investigated.

3.2 Dependency of the CO₂ reduction to formate on the conductivity at constant NaHCO₃ concentration

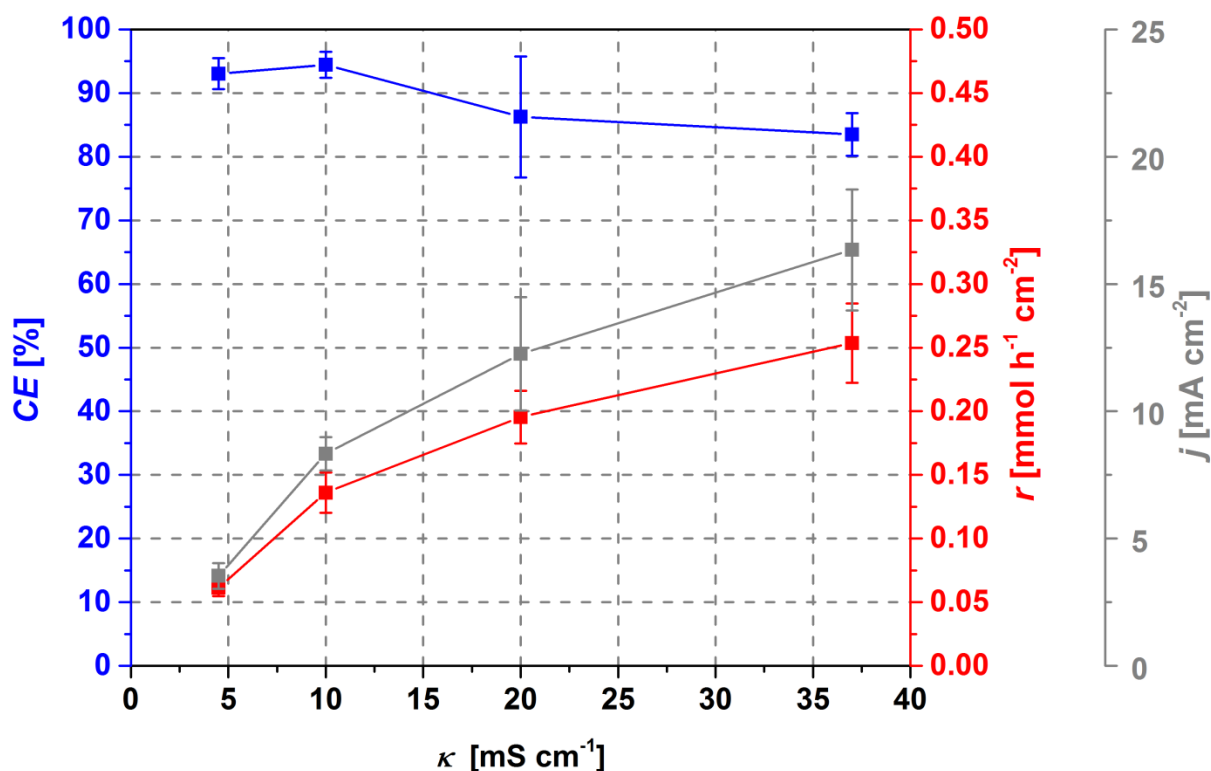


Figure 3: Dependence of the electrochemical CO₂ reduction to formate on the conductivity at constant NaHCO₃ concentration. Blue: coulombic efficiency (CE) and red: rate (r) of electrochemical CO₂ reduction to formate. All experiments were conducted in 0.05 mol L⁻¹ NaHCO₃ (pH 6.5) as electrolyte solution; κ of the electrolyte solution was adjusted by addition of Na₂SO₄; $n = 6$ except for $\kappa = 10$ mS cm⁻¹ $n = 3$. Reported values are mean values and the error bars represent the confidence interval ($\alpha = 0.05$).

An operational parameter of high practical relevance in electrochemical synthesis is the electrolyte conductivity, κ . It influences the availability of CO₂ (aq) by reducing its saturation concentration in solution, but also changes the acidity and dissociation constants of the carbonic acid system [32]. Conductivity will also influence the charge balancing and ion transfer at the electrode surface and within the bulk electrolyte solution of the electrochemical half cell [2, 44, 45]. Moreover, increasing κ also decreases internal resistance and hence the needed power input for the electrochemical operation (see section 3.4).

The conductivity of the electrolyte solution was adjusted by the addition of Na_2SO_4 as it is not affecting the pH and as it was also previously reported to be electrochemically inert at oxidative potentials [44].

Figure 3 shows that r increases with increasing κ while simultaneously the current density increases. For instance, by roughly doubling κ from 4.5 mS cm^{-1} to 10 mS cm^{-1} , r (from $0.061 \pm 0.007 \text{ mmol h}^{-1} \text{ cm}^{-2}$ to $0.136 \pm 0.016 \text{ mmol h}^{-1} \text{ cm}^{-2}$) and j (from $3.5 \pm 0.5 \text{ mA cm}^{-2}$ to $8.3 \pm 0.7 \text{ mA cm}^{-2}$) are more than doubled. In a range of up to 10 mS cm^{-1} the CE is not affected, which also proves that Na_2SO_4 is electrochemically inert at reductive potentials. Exceeding a certain conductivity between $10 \text{ mS cm}^{-1} < \kappa < 20 \text{ mS cm}^{-1}$ slightly decreases the CE from $\sim 95 \%$ to $\sim 85 \%$. This trend continues with statistical significance when further increasing κ up to 37 mS cm^{-1} .

However, increasing κ from 4.5 mS cm^{-1} to 37 mS cm^{-1} leads to improved space-time-yields as r increases by a factor of 3.9. This phenomenon was already observed for electroorganic synthesis at oxidative potentials [44]. Noteworthy, formate was the only analyte detected in the liquid phase. At κ of 37 mS cm^{-1} the formation of gas bubbles on the electrode surface was visible to the naked eye indicating increased gas formation. By GC-TCD measurements H_2 was identified as the only gaseous product (see Figure S5). Loss of In from the graphite backbone to the electrolyte solution causing the performance drop can be excluded as the amount of In in the electrolyte solution was only $3.3 \pm 1.4 \text{ }\mu\text{g}$. This equals 0.5% of the total In loading on the graphite backbone ($635 \text{ }\mu\text{g}$, see section 2.3.2) and is in the range of the amount of In detected in the electrolyte solution with lower κ (4.5 mS cm^{-1}) of experiments with different E_{WE} of -2.2 V and -3.0 V (see Figure 5, $1.1 \pm 1.3 \text{ }\mu\text{g}$ at -2.2 V and $6.1 \pm 8.7 \text{ }\mu\text{g}$ at -3.0 V , i.e. 0.2% and 1.0% of the total In loading on the graphite electrode backbone, respectively).

Briefly, increasing κ of the electrolyte solution by adding an electrochemically inert supporting electrolyte (here Na_2SO_4) increases the current densities and allows higher rates while only slightly decreasing the CE . This finding is highly interesting as increasing the NaHCO_3

concentration will also increase κ of the electrolyte solution and therefore could have similar effects on the space-time yields and the needed power input.

3.3 Dependency of the electrochemical CO₂ reduction to formate on the NaHCO₃ concentration at constant electrolyte conductivity

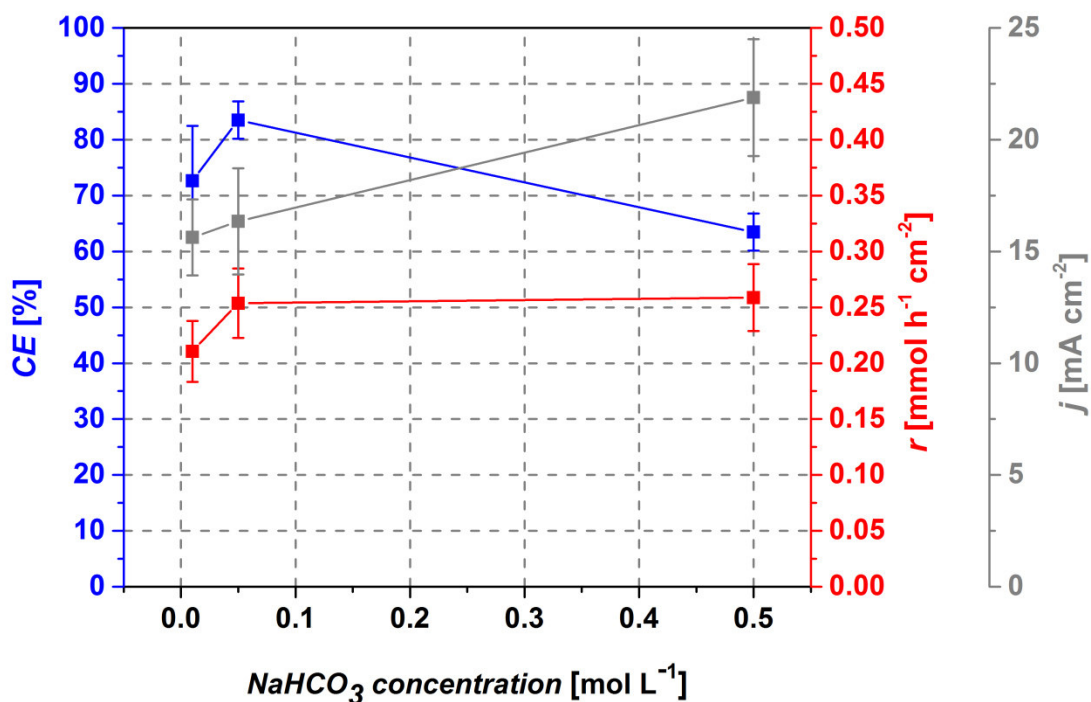


Figure 4: Dependence of the electrochemical CO₂ reduction to formate on the NaHCO₃ concentration. Blue: coulombic efficiency (*CE*) and red: rate (*r*) of electrochemical CO₂ reduction to formate. κ of the electrolyte solutions containing 0.01 mol L⁻¹ and 0.05 mol L⁻¹ were adjusted to $\kappa = 37$ mS cm⁻¹ by addition of Na₂SO₄ in order to match κ of the 0.5 mol L⁻¹ NaHCO₃ electrolyte solution; $n = 6$ except for 0.01 mol L⁻¹ NaHCO₃ $n = 5$. Reported values are mean values and the error bars represent the confidence interval ($\alpha = 0.05$).

The most frequently used electrolyte solution for electrochemical CO₂ reduction is aqueous KHCO₃ [2, 6, 7, 13, 34, 46-51]. Only in a few studies NaHCO₃ was applied as electrolyte solution [35, 52-55]. However, in all cases an equilibration according to Eq. (3) to (6) of the carbonate species will take place and the higher the HCO₃⁻ and CO₃²⁻ concentration the higher is the conductivity. In order to study the effect of the NaHCO₃ concentration

independently from κ , electrolyte solutions containing 0.01 mol L⁻¹ and 0.05 mol L⁻¹ NaHCO₃ were adjusted to 37 mS cm⁻¹ by addition of Na₂SO₄ in order to match κ of the 0.5 mol L⁻¹ NaHCO₃ electrolyte solution. Noteworthy, the aqueous solutions are concentrated and hence the properties and equilibration kinetics of the carbonic species differ from ideal solutions and resemble the processes found in marine systems [31, 32]. The pH of these solutions was measured before and after CO₂ bubbling, and a strong effect of CO₂ bubbling was found being the lowering of the pH from values as high as 9.4 to values as low as 5.8 (see Table 1 and Table S5). Interestingly, using kinetic modeling of the CO₂ bubbling shows that the freshly prepared solutions with higher pH possess only low amounts of dissolved CO₂, as most of the carbon introduced *via* NaHCO₃ is present as HCO₃⁻ and CO₃²⁻ species (see Table S5 and Figure S7). When CO₂ is bubbled in these solutions, it leads to a re-balancing of the equilibria of the dissolved species (see Eq. (3) to (6)), up to the saturation concentration of CO₂ (aq). As expected, this lowers the pH and affects the ratio between the HCO₃⁻ and CO₃²⁻: HCO₃⁻ concentration increases, and the CO₃²⁻ concentration decreases. In all cases the electrolyte solution, serves also as a carbon storage from bubbling of CO₂. The model shows the accumulation of additional 29.3 mM, 46.2 mM and 349.6 mM (for the 0.01, 0.05 and 0.5 mol L⁻¹ electrolyte solutions respectively, see Table S5) total carbon, as it has also experimentally been previously shown by Zhong *et al.* [27]. Noteworthy, the shifts in pH measured before and after formate production (see Table 1) are induced by the electrode reactions (see Eq. (1) and Eq. (2)), as no pH shifts occurred when the electrolyte solution was only purged with CO₂ for 60 min at open circuit potential (see Figure S6).

At a E_{WE} of -2.2 V an increase in initial NaHCO₃ concentration from 0.01 mol L⁻¹ to 0.05 mol L⁻¹ leads only to a low, but significant increases of r which stagnates when further increasing the initial NaHCO₃ concentration of the electrolyte solution to 0.5 mol L⁻¹ (see Figure 4), although the current density is continuously increasing over the whole NaHCO₃ concentration range. Hence, the selectivity, S , and the CE are strongly influenced by NaHCO₃ concentration. While there is an increase of the CE when the initial NaHCO₃ concentration

was increased from 0.01 mol L⁻¹ to 0.05 mol L⁻¹ it decreased from ≈ 84 % to ≈ 72 % when using initially 0.5 mol L⁻¹ NaHCO₃. When considering the initial 0.05 mol L⁻¹ NaHCO₃ as point of reference, one explanation for the decrease in *CE* when lowering the NaHCO₃ concentration to initially 0.01 mol L⁻¹ might be the more acidic pH (see Table 1) promoting the HER [56]. In contrast, the *CE* drop when using an initial concentration of 0.5 mol L⁻¹ cannot be attributed to the same reason. Nevertheless, in all experiments H₂ was the only side product (see Figure S5) and the e⁻-balance was closed.

Research on the effects of KHCO₃ concentration on the electrochemical CO₂ reduction has been recently published by Zhong *et al.* [6]. They observed similar behavior of a strong dependency on KHCO₃ concentration for the formation of gaseous products from electrochemical CO₂ reduction on Cu electrodes in the range from 0.01 M to 1.5 M KHCO₃ resulting a similar pH range compared to the present study. The maximum *CE* of the production of carbon-based products of 43.7 % was reached at a relative low concentration of 0.1 M KHCO₃. They hypothesized that this is caused by the K⁺, originating from the KHCO₃ solution used in their study, which are drawn electrostatically to the electrode and thereby block the electrode surface for the non-polar CO₂ molecules supposed to serve as reactant. Contrary, H⁺, due to their small size and Grothuss mechanism based transport [57], are not affected while CO₂ molecules are diffusion limited [6]. Indeed, in this study with increasing NaHCO₃ concentration *r*_{H₂} and *CE*_{H₂} significantly increased (see Figure 5) which is supported by the visual observation of gas bubble formation on the electrode surface. However, the concentration of Na⁺ in the 0.05 M NaHCO₃ electrolyte adjusted to 37 mS cm⁻¹ was higher than in the 0.5 M NaHCO₃ electrolyte (37 mS cm⁻¹) due to the adjustment of *κ* by using Na₂SO₄ (see Table 1). Hence, we conclude that Na⁺ is not causing the *CE* decrease. Of course it has to be noted that Zhong *et al.* used KHCO₃ (instead of NaHCO₃) but the Stokes radius of hydrated Na⁺ is larger than that of K⁺ (1.94 Å vs. 1.34 Å) [58] which we suppose to additionally increase the effect of electrode surface blocking. Additionally, we

hypothesize that the increased concentration of HCO_3^- as proton source ($\text{p}K_a = 6.35$, see Eq. (5)) itself is the reason for the increased r_{H_2} and CE_{H_2} because its higher proton-donating ability in comparison to pure water ($\text{p}K_a = 14$) [26, 35]. This is supported by the model which reveals that in 0.5 M NaHCO_3 solution the HCO_3^- concentration is more than 10 times higher than in the 0.05 M NaHCO_3 solution (see Table S5). Furthermore, the concentration of HCO_3^- as proton source in both solutions increases over the formate production period of 1 h which possibly intensifies the effect (see Table S5). The instability of the In coating by corrosion or spalling off of the In from the graphite electrode backbone by H_2 gas bubble formation has to be taken into account. After 1 h of operation $20.2 \pm 2.6 \mu\text{g}$ of In were detected within the electrolyte solution. This equals 3.2 % of the total In loading on the graphite backbone ($635 \mu\text{g}$) and is about six times higher than the amount of In detected in an electrolyte solution with the same κ and applied E_{WE} but with just 0.05 M NaHCO_3 (see Figure 5). Hence, in this experiment the loss of In from the electrode backbone might contribute to the observed performance drop.

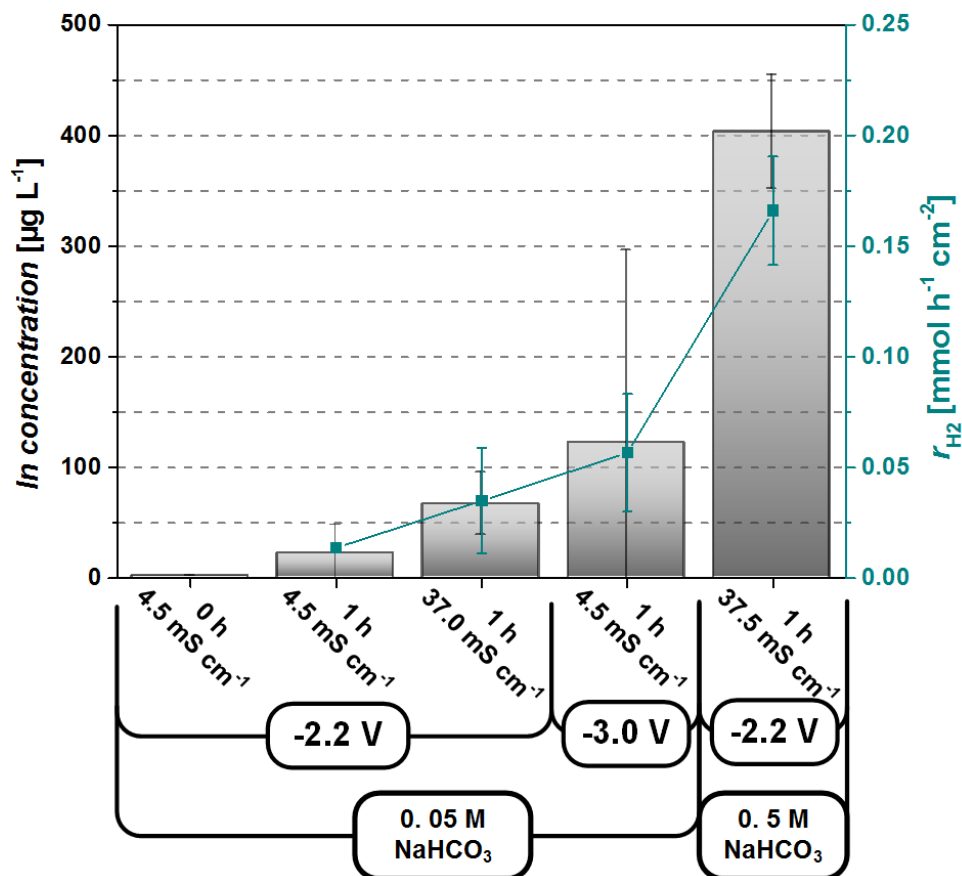


Figure 5: Loss of In from the graphite electrode backbone to the electrolyte solution in correlation with the average r_{H_2} depending on applied E_{WE} , electrolyte solution conductivity, κ , and NaHCO_3^- concentration. $n = 3$ except for 0.05 M NaHCO_3 electrolyte solution with $\kappa = 10 \text{ mS cm}^{-1}$ at -2.2 V $n = 4$. Reported values are mean values and the error bars represent the confidence interval ($\alpha = 0.05$).

3.4 Power input and selectivity of In-based electrochemical CO₂ reduction to formate

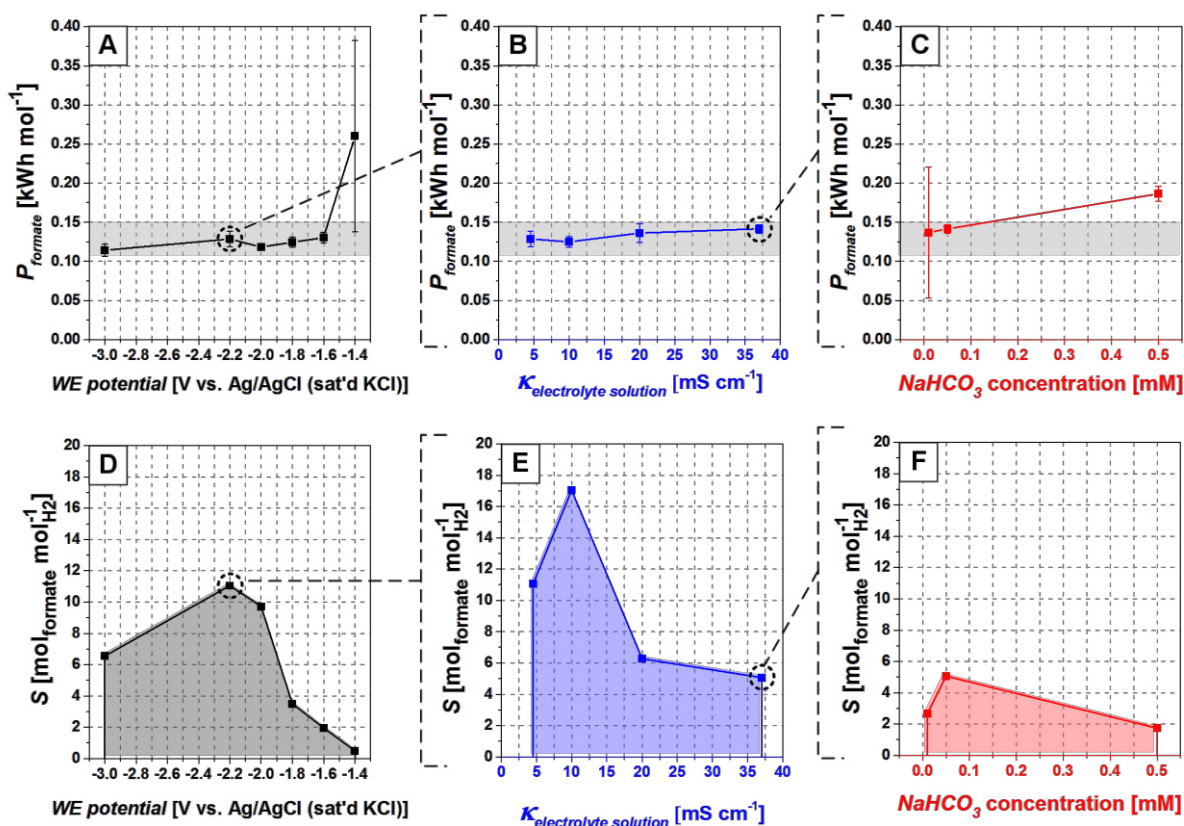


Figure 6: Power input (A to C) and average selectivity (S) for formate production (D to F) as function of applied E_{WE} ; electrolyte solution conductivity and NaHCO₃ concentration. The grey area in Figure A to C indicates the interquartile range of the half cell power input which can be reached with the electrochemical cell ($n = 69$). The colored areas under the curves in Figure D to F are introduced to increase the clarity of the changes in selectivity; $n = 6$ except for $\kappa = 10 \text{ mS cm}^{-1}$ with $n = 3$ and $0.01 \text{ mol L}^{-1} \text{ NaHCO}_3$, $n = 5$. Reported values for Figure A to C are mean values and the error bars represent the confidence interval ($\alpha = 0.05$).

In the following the impact of the above discussed process parameters on the required power input (based on the cathodic half cell) per produced mole formate, P_{formate} , and on the selectivity, S , of the formate production is assessed and depicted in Figure 6. It has to be noted that for the required power input only trends can be assessed, as specific numbers are dependent on the geometry of the electrode and the electrochemical reactor itself as well as the anode reaction, which may create an additional valuable product.

At E_{WE} of -1.4 V the power input needed ($0.25 \text{ kWh mol}^{-1}_{\text{formate}}$) is almost twice the power input at E_{WE} of -1.6 V. A further E_{WE} decrease does not affect the required power input being in the range between $0.11 \text{ kWh mol}^{-1}_{\text{formate}}$ and $0.15 \text{ kWh mol}^{-1}_{\text{formate}}$ (see grey area in Figure 6 A to C).

At E_{WE} of -2.2 V the increase of κ from 4.5 mS cm^{-1} to 37 mS cm^{-1} only slightly affects the power demand by an increase from $0.129 \text{ kWh mol}^{-1}_{\text{formate}}$ to $0.142 \text{ kWh mol}^{-1}_{\text{formate}}$ (see Figure 6 B). This is in contrast to the impact of NaHCO_3 concentration at constant κ . The required power input per mol formate increased significantly by 30 %, i.e. to $0.190 \text{ kWh mol}^{-1}_{\text{formate}}$, when increasing the initial NaHCO_3 concentration from 0.05 M to 0.5 M (see Figure 6 C).

When evaluating the selectivity for formate production over the HER, the picture looks different. Clearly, at E_{WE} of -2.2 V the highest selectivity for formate production of $S = 11.0$ was reached (see Figure 6 D) which of course reflects also the trend found for the CE that was already discussed in section 3.1. When applying $E_{WE} = -2.2 \text{ V}$, S could be further increased to $S = 17.0$ for a 0.05 M NaHCO_3 electrolyte solution by adjusting κ to 10 mS cm^{-1} (see Figure 6 E). At higher κ of the electrolyte solution S drastically decreased. In turn, when using an electrolyte solution with high κ (37 mS cm^{-1}) an improved S was reached at very low initial NaHCO_3 concentration of 0.05 M (see Figure 6 F). This selectivity ($S = 5$) was, however, below the values that can be reached at the same NaHCO_3 concentration but at lower conductivity ($S = 17$, Figure 6 E and F). The maximum value for the selectivity of $S = 17$ is even higher than the one reported for Sn-based gas diffusion electrodes of $S \approx 4.6$ after 1 h [13].

The results show that the E_{WE} is the most important parameter but at the same time the power input for formate production is constant over a wide range. The selectivity of the electrochemical CO_2 reduction to formate in turn is strongly influenced by the conductivity and the HCO_3^- concentration of the electrolyte solution. Zhong *et al.* assumed that low concentration of HCO_3^- , i.e. below 0.1 M, is beneficial for improving CE of carbon-based

products but is limited by κ [6]. This problem can be circumvented by the addition of electrochemically inert supporting electrolyte, e.g. Na_2SO_4 . However, this study also points out that the HCO_3^- concentration should not fall below a critical value as, due to the equilibrium reactions (see Eq. (3) to (6)), it is also serving as a reservoir for CO_2 and H^+ [2]. Experimentally determined this critical concentration is 0.05 M HCO_3^- being well in accordance with the modeling suggesting it to be between 0.057 M and 0.070 M HCO_3^- (see Table S5).

3.5 Influence of O_2 on the electrochemical CO_2 reduction to formate

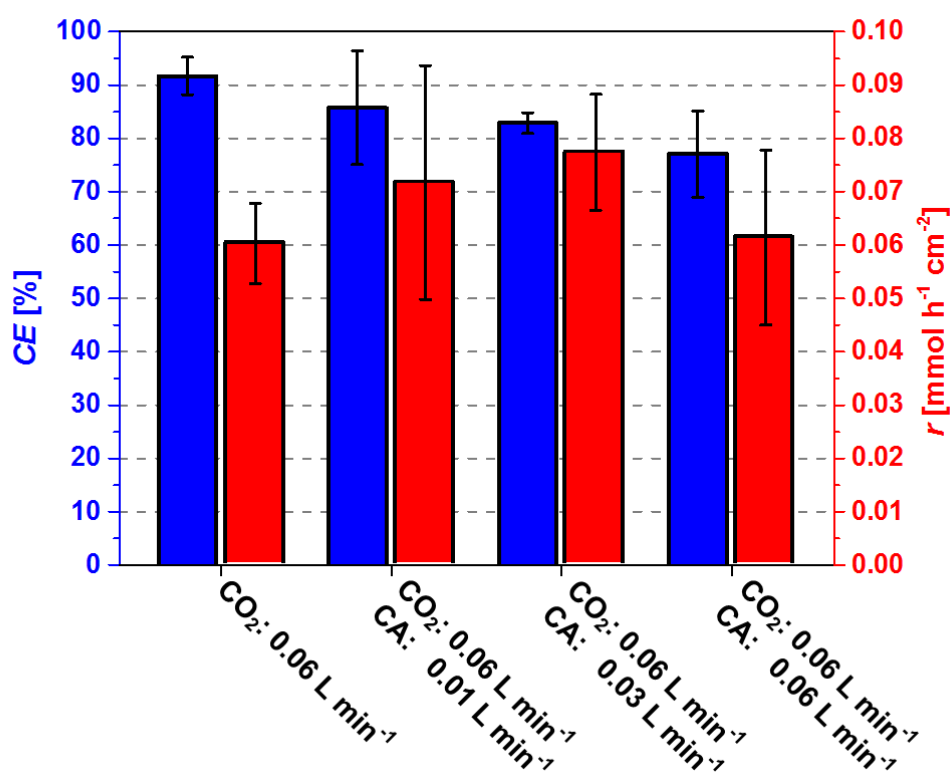


Figure 7: Influence of oxygen on the electrochemical CO_2 reduction to formate at In electrodes. The x-axis caption describes the volumetric gas flow of CO_2 (v_{CO_2}) and compressed air (v_{CA}). Blue bars: coulombic efficiency (CE) and red bars: rate (r) of electrochemical CO_2 reduction to formate. All experiments were conducted in 0.05 mol L⁻¹ NaHCO_3 (pH 6.5) as electrolyte solution with $\kappa = 4.5 \text{ mS cm}^{-1}$; $n = 3$ except for the experiment of only gassing with CO_2 with $n = 6$. Reported values are mean values and the error bars represent the confidence interval ($\alpha = 0.05$).

Table 2: Ratio of the volumetric gas flow of CO₂ (v_{CO_2}) to compressed air (v_{CA}), the resulting gas composition, and the pH at the beginning and the end of the respective experiment.

Ratio of volumetric gas flow $v_{CO_2} : v_{CA}$ [L _{CO₂} min ⁻¹ : L _{CA} min ⁻¹]	Gas composition [mol-% _{CO₂} : mol-% _{N₂} : mol-% _{O₂}]	pH _{Start}	pH _{End}
0.06 : 0.00	98.5 : 0.2 : 0.1	6.5	6.6
0.06 : 0.01	85.6 : 11.1 : 3.0	6.9	6.7
0.06 : 0.03	68.6 : 23.9 : 6.4	6.9	6.8
0.06 : 0.06	48.6 : 39.6 : 10.6	6.9	6.9

A high selectivity for the electrochemical CO₂ reduction to formate based on In as electrocatalyst has been shown in this study. However, previously we have shown that it is also prone to mixed-potential formation by the presence of phosphate salts, yeast extract and trace elements being typical components of microbial media [17]. The presence of O₂ in the electrolyte solution can also cause mixed-potential formation due to oxygen reduction at the cathode, leading to internal parasitic currents [59] effecting *S* and *CE*.

A potential source for O₂ might be the transport of O₂ produced at the anode ($H_2O \rightarrow \frac{1}{2} O_2 + 2H^+ + 2e^-$) through the membrane to the cathode. Even more relevant is considering formate utilization by *in situ* biosynthesis for which also aerobic conditions can be advantageous. In order to characterize the influence of O₂ on the CO₂ reduction the catholyte was purged with gas mixtures of varying volumetric gas flow ratios of CO₂ and compressed air (see Table 2). The results are depicted in Figure 7.

Surprisingly, the effect of O₂ on the performance of electrochemical CO₂ reduction to formate is only minor at the conditions studied. Regarding the *CE* there is a trend towards a decrease for higher O₂ concentrations. This becomes only significant for an O₂ concentration of 6.4 mol-% and 10.6 mol-% when compared to the standard conditions (off gas: 98.5 mol-%_{CO₂} : 0.2 mol-%_{N₂} : 0.1 mol-%_{O₂}). Nevertheless, although the O₂ concentration was raised

by the factor 64 and 106, respectively, the *CE* drops only from 91.7 % (at standard conditions) to 82.9 % and 77.1 % for 6.4 mol-% and 10.6 mol-%, respectively. Even more surprising and important is that *r* is not significantly affected by the presence of O₂. To the best of our knowledge the O₂ influence on the electrochemical CO₂ reduction has been addressed in this study for the first time.

The most important possible “parasitic” process explaining the observed trend for the *CE* is the e⁻ scavenging by electrochemical reduction of the O₂ to OH⁻ ($\frac{1}{2} \text{O}_2 + \text{H}_2\text{O} + 2 \text{e}^- \rightarrow 2 \text{OH}^-$). OH⁻ subsequently reacts with CO₂ to form HCO₃⁻ [1] again serving as CO₂ reservoir. The formation of HCO₃⁻ would be accompanied by the manifestation of a more alkaline pH over the period of the experiment. Comparing the pH at the beginning and the end of the experiment (see Table 2), however, this was not detected within the timeframe of the 1 h experiment.

It has to be noted that introducing N₂ and O₂ to the gas stream causes an increase of the initial pH of the electrolyte solution compared to pure CO₂ purging from 6.5 to 6.9 (see Table 2). This is due to the decrease of the CO₂ partial pressure of the gas stream. As a result, the ratio of CO₂/HCO₃⁻ in the electrolyte solution is lower at the start of the experiment compared to the standard conditions. As already shown in section 3.3 at ratios of CO₂/HCO₃⁻ lower than 0.39 ([mol_{CO₂} mol⁻¹_{HCO₃⁻], cf. Figure 4 and Figure S7 B) the *CE* is negatively affected, which is here caused by the decreased partial pressure of CO₂.}

3.7 Implications for application of *in situ* formate production in an electrobiorefinery

The product of the electrochemical CO₂ reduction gained in this study with high *r*, *CE* and *S* is formate. Formate exhibits a high solubility, low cytotoxicity and serves not only as e⁻ shuttle between cathode and microorganisms but also as a carbon source [10, 20]. Nevertheless, the high solubility of formate increases the costs for the separation from the electrolyte solution. Therefore, it is appealing to perform the electrochemical CO₂ reduction to formate *in situ* in a secondary MET meaning seizing its microbial metabolization to value-added

products in an integrated system facing the same process media [17, 20, 22]. Noteworthy, H₂ was the only side product detected that can also be valorized as it serves as electron donor for microorganisms [60, 61].

As shown above, when applying a E_{WE} of -1.6 V to -3.0 V a constant power input of $\approx 0.123 \text{ kWh mol}^{-1}_{\text{formate}}$ is needed (see section 3.4). Although the E_{WE} is an operational parameter influencing the CE as well as r , the results also highlight the flexibility of formate production. E_{WE} can be used to adjust S , and therewith also the ratio of the two microbial e-donors formate and H₂. This becomes especially interesting when formate is produced as microbial substrate (carbon source and/or e-donor) but an additional e-donor is necessary in order to improve the thermodynamic feasibility of the biosynthesis. Therefore, the potential can be used to steer S and hence the performance of the secondary MET. Thus, it can be an advantage working at different potentials for different process phases, e.g. for biomass buildup and biotransformation.

The conductivity of the electrolyte solutions plays a crucial role for the selectivity of formate production that can be adjusted by the addition of electrochemically inert supporting electrolyte [44]. Furthermore, with the view to the microbial component in a secondary MET the high salinity has to be considered as a possible stress factor for the microorganisms, and in case of using microbial mixed cultures (microbiomes) also as a selection factor [62]. In this study, electrochemically inert Na₂SO₄ was used. Applying -2.2 V in low concentrated 0.05 M NaHCO₃ electrolyte solution, by far the highest selectivity for formate production was reached at a κ of 10 mS cm⁻¹ accompanied by the benefit of a slight reduction of the power input. Typical salt concentrations used in electrochemical cells are in the range of, for example, 0.5 M Na₂SO₄ ($\approx 71 \text{ g L}^{-1}$) resulting in a conductivity of 64 mS cm⁻¹ (at 30°C) [63]. However, in order to adjust the conductivity to the optimum value of 10 mS cm⁻¹ for highly selective formate production, an amount of $\approx 5.3 \text{ g L}^{-1}$ Na₂SO₄ is necessary (see Figure S8). A study by Sydow *et al.* [63] was devoted to the optimization of the electrolyte solution in bioelectrochemical systems for allowing growth of *Cupriavidus necator*, being a potential

formatotrophic and hydrogenotrophic biocatalyst, as well as to enable high electrochemical performance. They increased the conductivity of the electrolyte solution up to 9.5 mS cm^{-1} , which is in the range of the optimum conductivity for electrochemical CO_2 reduction to formate, observed in the present study.

When now assuming a microorganism consuming formate at a rate of $1 \text{ g L}^{-1} \text{ h}^{-1}$ and applying the formate production rate r reached at optimal κ of 10 mS cm^{-1} at -2.2 V ($0.136 \pm 0.016 \text{ mmol h}^{-1} \text{ cm}^{-2}$) the electrode in a 1 L bioreactor must possess a surface area of 0.016 m^2 . This electrode surface area is already one order of magnitude smaller compared to our previous study [17]. Although deactivation during long-term use is still neglected in this calculation a flat metal electrode with the mentioned surface area would already fit into a 1 L bioreactor. Beyond that, considering the use of 3D electrode materials, e.g. reticulated vitreous carbon exposing a specific surface area of $6.5 \text{ m}^2 \text{ dm}^{-3}$ [64], such an electrode would occupy a volume of 0.0025 dm^3 . This equals only one four hundredth (0.0025 L) of the available volume within a 1 L bioreactor.

Further increase of the conductivity up to 37 mS cm^{-1} leads to increased r but at the cost of a significantly elevated power input of $0.142 \text{ kWh mol}^{-1}_{\text{formate}}$, as the selectivity for formate production decreases. The same holds true for high NaHCO_3 concentrations leading to high conductivities (see Figure 6). Independent from κ the optimal NaHCO_3 concentration is reached around 0.05 M NaHCO_3 resulting in a mild biocompatible pH of 6.5. Surprisingly, the influence of O_2 on the electrochemical CO_2 reduction to formate is quite low being an interesting finding as it shows that a secondary MET approach is not limited to the cultivation of anaerobic microorganisms. Further the energy demand for the supplementation of O_2 to the electrolyte solution can be reduced by recycling O_2 that is produced at the anode.

It has to be noted that the increase of r , r_{H_2} and CE_{H_2} and the slight decrease in CE and S positively correlate with the amount of In lost during the experiment (see Figure 5). Although the amount of In in the electrolyte solution was still low, this points into the direction that a physical loss of the In electrocatalyst is accelerated at higher rates. This shifts the selectivity

to HER over time and in turn leads to even more pronounced spalling off of the In catalyst from the electrode backbone by H₂ gas bubble formation. High area specific formate production rates (e.g. high current densities) can be circumvented by an appropriate specific surface area of the electrode using 3D electrodes. This will also improve long-term operation of CO₂ reduction to formate in secondary METs. Furthermore, at too high concentrations formate is shown to be cytotoxic [65, 66]. Demand-driven and gradientless formate production along the height of fluid column within the reactor therefore is of high importance in order to avoid metabolic inhibition. As shown in the present study electrochemical CO₂ reduction meets this challenge as especially space-time yields of formate production can be steered.

4. Conclusion

Based on the high reproducibility of the used experimental setup the effects of key process parameters on the electrochemical CO₂ reduction to formate using In as electrocatalyst were quantified with statistical significance. E_{WE} is demonstrated to be the main parameter for steering CE , S and r of formate production as well as determining the required power input (considering the cathodic half-cell). The conductivity of the electrolyte solution is a further process parameter to boost S and r . Surprisingly, the adjustment of the electrolyte solution by varying NaHCO₃ did not lead to an improvement of the process performance indicating that HCO₃⁻ has a minor role in the electrochemical CO₂ reduction to formate but is rather serving as a reservoir for the reactant CO₂ and H⁺. In contrast, using Na₂SO₄ to adjust the conductivity is promising as it is electrochemically inert at reductive conditions. Based on a kinetic model it was revealed that CO₂ sparging of the electrolyte solution introduces extra carbon to the system. Furthermore the model described the experimentally observed changes in pH during the formate production leading to re-balancing of the different carbonaceous species in the electrolyte solution. The model therefore might be suitable to

estimate reasonable rates of CO₂ supply regarding the formate production rates in order to tailor the gas-stream and reduce the energy input for the CO₂ sparging.

However, the process performance is limited by the stability of the In coating on the electrode backbone at high formate production rates. The highest selectivity towards formate production was found at moderate Na₂SO₄ concentration and NaHCO₃ concentration at near neutral pH meeting biocompatible conditions. This includes also aerobic conditions as the impact on the formate production by the presence of O₂ in the electrolyte solution is remarkably low. Even at these conditions the reached formate production rates by electrochemical CO₂ reduction match microbial formate consumption rates of pure cultures. High-surface area 3D electrode materials can further increase r showing the flexibility of the proposed concept.

These findings demonstrate that the coupling of electrochemical CO₂ reduction to formate with its subsequent *in situ* biotransformation to value-added products in a secondary MET can become technologically relevant and an important component of a sustainable economy.

Acknowledgements

We thank Jürgen Steffen, Ines Volkmann, and Dr. Hans-Joachim Stärk for ICP-MS analysis (Helmholtz Centre for Environmental Research GmbH - UFZ, Department of Analytical Chemistry, Leipzig, Germany). F.H. acknowledges support by the BMBF (Research Award “Next generation biotechnological processes - Biotechnology 2020+”) and the Helmholtz-Association (Young Investigators Group). This work was supported by the Helmholtz-Association within the Research Programme Renewable Energies. There is no conflict of interests.

References

- [1] T. Haas, R. Krause, R. Weber, M. Demler, G. Schmid, Technical photosynthesis involving CO₂ electrolysis and fermentation, *Nat. Catal.*, 1 (2018) 32-39.
- [2] J.L. White, A.B. Bocarsly, Enhanced Carbon Dioxide Reduction Activity on Indium-Based Nanoparticles, *J. Electrochem. Soc.*, 163 (2016) H410-H416.
- [3] WMO Greenhouse Gas Bulletin: The State of Greenhouse Gases in the Atmosphere Based on Global Observations through 2016, World Meteorological Organization, 2017, pp. 1-8.
- [4] J.G.J. Olivier, G. Janssens-Maenhout, M. Muntean, J.A.H.W. Peters, Trends in global CO₂ emissions 2016, PBL Netherlands Environmental Assessment Agency, European Commission Joint Research Centre, Den Haag, 2016, pp. 1-86.
- [5] W. Luc, C. Collins, S. Wang, H. Xin, K. He, Y. Kang, F. Jiao, Ag-Sn Bimetallic Catalyst with a Core-Shell Structure for CO₂ Reduction, *J. Am. Chem. Soc.*, 139 (2017) 1885-1893.
- [6] H. Zhong, K. Fujii, Y. Nakano, Effect of KHCO₃ Concentration on Electrochemical Reduction of CO₂ on Copper Electrode, *J. Electrochem. Soc.*, 164 (2017) F923-F927.
- [7] K.P. Kuhl, E.R. Cave, D.N. Abram, T.F. Jaramillo, New insights into the electrochemical reduction of carbon dioxide on metallic copper surfaces, *Energy Environ. Sci.*, 5 (2012) 7050-7059
- [8] J. Wu, S. Ma, J. Sun, J.I. Gold, C. Tiwary, B. Kim, L. Zhu, N. Chopra, I.N. Odeh, R. Vajtai, A.Z. Yu, R. Luo, J. Lou, G. Ding, P.J.A. Kenis, P.M. Ajayan, A metal-free electrocatalyst for carbon dioxide reduction to multi-carbon hydrocarbons and oxygenates, *Nat. Commun.*, 7 (2016) 13869-13875.
- [9] M. Shemfe, S. Gadkari, E. Yu, S. Rasul, K. Scott, I.M. Head, S. Gu, J. Sadhukhan, Life cycle, techno-economic and dynamic simulation assessment of bioelectrochemical systems: A case of formic acid synthesis, *Bioresour. Technol.*, 255 (2018) 39-49.
- [10] A. Bar-Even, E. Noor, A. Flamholz, R. Milo, Design and analysis of metabolic pathways supporting formatotrophic growth for electricity-dependent cultivation of microbes, *Biochim. Biophys. Acta*, 1827 (2013) 1039-1047.
- [11] Chemical Economics Handbook: Formic Acid, CEH Marketing Research Report, IHS Markit, 2016.
- [12] N.M. Aslam, M.S. Masdar, S.K. Kamarudin, W.R.W. Daud, Overview on Direct Formic Acid Fuel Cells (DFAFCs) as an Energy Sources, *APCBEE Procedia*, 3 (2012) 33-39.
- [13] D. Kopljär, N. Wagner, E. Klemm, Transferring Electrochemical CO₂ Reduction from Semi-Batch into Continuous Operation Mode Using Gas Diffusion Electrodes, *Chem. Eng. Technol.*, 39 (2016) 2042-2050.
- [14] A. Boddien, C. Federsel, P. Sponholz, D. Mellmann, R. Jackstell, H. Junge, G. Laurenczy, M. Beller, Towards the development of a hydrogen battery, *Energy Environ. Sci.*, 5 (2012) 8907-8911.
- [15] U. Eberle, M. Felderhoff, F. Schüth, Chemical and physical solutions for hydrogen storage, *Angew. Chem. Int. Ed.*, 48 (2009) 6608-6630.

- [16] F. Studt, M. Behrens, E.L. Kunkes, N. Thomas, S. Zander, A. Tarasov, J. Schumann, E. Frei, J.B. Varley, F. Abild-Pedersen, J.K. Nørskov, R. Schlögl, The Mechanism of CO and CO₂ Hydrogenation to Methanol over Cu-Based Catalysts, *ChemCatChem*, 7 (2015) 1105-1111.
- [17] C. Gimkiewicz, R. Hegner, M.F. Gutensohn, C. Koch, F. Harnisch, Study of Electrochemical Reduction of CO₂ for Future Use in Secondary Microbial Electrochemical Technologies, *ChemSusChem*, 10 (2017) 958-967.
- [18] P. Anastas, J.C. Warner, *Green Chemistry: Theory and Practice*, 6th ed., Oxford University Press, Oxford, 1998.
- [19] A. Bar-Even, Formate Assimilation: The Metabolic Architecture of Natural and Synthetic Pathways, *Biochemistry*, 55 (2016) 3851-3863.
- [20] H. Li, P.H. Opgenorth, D.G. Wernick, S. Rogers, T.Y. Wu, W. Higashide, P. Malati, Y.X. Huo, K.M. Cho, J.C. Liao, Integrated electromicrobial conversion of CO₂ to higher alcohols, *Science*, 335 (2012) 1596.
- [21] F. Harnisch, C. Urban, Electrobiorefineries: Unlocking the synergy of electrochemical and microbial conversions, *Angew. Chem. Int. Ed.*, (2017) [doi: 10.1002/anie.201711727].
- [22] U. Schröder, F. Harnisch, L.T. Angenent, Microbial electrochemistry and technology: terminology and classification, *Energy Environ. Sci.*, 8 (2015) 513-519.
- [23] C. Urban, J. Xu, H. Sträuber, T.R. dos Santos Dantas, J. Mühlenberg, C. Härtig, L.T. Angenent, F. Harnisch, Production of drop-in fuels from biomass at high selectivity by combined microbial and electrochemical conversion, *Energy Environ. Sci.*, (2017).
- [24] M. Suastegui, J.E. Matthiesen, J.M. Carraher, N. Hernandez, N. Rodriguez Quiroz, A. Okerlund, E.W. Cochran, Z. Shao, J.P. Tessonier, Combining Metabolic Engineering and Electrocatalysis: Application to the Production of Polyamides from Sugar, *Angew. Chem. Int. Ed.*, 55 (2016) 2368-2373.
- [25] M. Azuma, K. Hashimoto, M. Hiramoto, M. Watanabe, T. Sakata, Electrochemical Reduction of Carbon Dioxide on Various Metal Electrodes in Low-Temperature Aqueous KHCO₃ Media, *J. Electrochem. Soc.*, 137 (1990) 1772.
- [26] C.W. Lee, N.H. Cho, K.D. Yang, K.T. Nam, Reaction Mechanisms of the Electrochemical Conversion of Carbon Dioxide to Formic Acid on Tin Oxide Electrodes, *ChemElectroChem*, 4 (2017) 2130-2136.
- [27] H. Zhong, K. Fujii, Y. Nakano, F. Jin, Effect of CO₂ Bubbling into Aqueous Solutions Used for Electrochemical Reduction of CO₂ for Energy Conversion and Storage, *J. Phys. Chem. C*, 119 (2015) 55-61.
- [28] R.E. Zeebe, D. Wolf-Gladrow, *CO₂ in Seawater: Equilibrium, Kinetics, Isotopes*, 1st ed., Elsevier Science, Amsterdam, 2001.
- [29] K. Al-Anezi, N. Hilal, Effect of Carbon Dioxide in Seawater on Desalination: A Comprehensive Review, *Sep. Purif. Rev.*, 35 (2006) 223-247.
- [30] F.J. Millero, The marine inorganic carbon cycle, *Chem. Rev.*, 107 (2007) 308-341.

- [31] K.G. Schulz, U. Riebesell, B. Rost, S. Thoms, R.E. Zeebe, Determination of the rate constants for the carbon dioxide to bicarbonate inter-conversion in pH-buffered seawater systems, *Mar. Chem.*, 100 (2006) 53-65.
- [32] W. Stumm, J.J. Morgan, *Aquatic chemistry: An introduction emphasizing chemical equilibria in natural waters*, Wiley-Interscience, New York, London, Sydney, Toronto, 1970.
- [33] Y. Hori, A. Murata, R. Takahashi, Formation of hydrocarbons in the electrochemical reduction of carbon dioxide at a copper electrode in aqueous solution, *J. Chem. Soc., Faraday Trans. 1*, 85 (1989) 2309-2326
- [34] Z.M. Detweiler, J.L. White, S.L. Bernasek, A.B. Bocarsly, Anodized indium metal electrodes for enhanced carbon dioxide reduction in aqueous electrolyte, *Langmuir*, 30 (2014) 7593-7600.
- [35] S. Zhang, P. Kang, T.J. Meyer, Nanostructured tin catalysts for selective electrochemical reduction of carbon dioxide to formate, *J. Am. Chem. Soc.*, 136 (2014) 1734-1737.
- [36] W. Lv, J. Zhou, F. Kong, H. Fang, W. Wang, Porous tin-based film deposited on copper foil for electrochemical reduction of carbon dioxide to formate, *Int. J. Hydrog. Energy*, 41 (2016) 1585-1591.
- [37] S. Kaneco, R. Iwao, K. Iiba, S. Itoh, K. Ohta, T. Mizuno, Electrochemical reduction of carbon dioxide on an indium wire in a KOH/methanol-based electrolyte at ambient temperature and pressure, *Environ Eng Sci*, 16 (1999) 131-137.
- [38] Y. Hori, Electrochemical CO₂ Reduction on Metal Electrodes, in: C.G. Vayenas, R.E. White, M.E. Gamboa-Aldeco (Eds.) *Modern Aspects of Electrochemistry*, Springer, New York, NY, 2008, pp. 89-189.
- [39] Y. Hori, S. Suzuki, Electrolytic Reduction of Carbon Dioxide at Mercury Electrode in Aqueous Solution, *Bull. Chem. Soc. Jpn.*, 55 (1982) 660-665.
- [40] S.D. Babenko, V.A. Benderskii, A.G. Krivenko, V.A. Kurmaz, Photocurrent kinetics at the electron emission from a metal into electrolyte solution, *J. Electroanal. Chem. Interfacial Electrochem.*, 159 (1983) 163-181.
- [41] D.J. Schiffrin, Application of the photo-electrochemical effect to the study of the electrochemical properties of radicals: CO₂ and CH₃, *Faraday Discuss. Chem. Soc.*, 56 (1973) 75-95.
- [42] W. Paik, T.N. Andersen, H. Eyring, Kinetic studies of the electrolytic reduction of carbon dioxide on the mercury electrode, *Electrochim. Acta*, 14 (1969) 1217-1232.
- [43] S. Kapusta, N. Hackerman, The Electroreduction of Carbon-Dioxide and Formic-Acid on Tin and Indium Electrodes, *J. Electrochem. Soc.*, 130 (1983) 607-613.
- [44] C. Stang, F. Harnisch, The Dilemma of Supporting Electrolytes for Electroorganic Synthesis: A Case Study on Kolbe Electrolysis, *ChemSusChem*, 9 (2016) 50-60.
- [45] D. Kopljar, A. Inan, P. Vindayer, N. Wagner, E. Klemm, Electrochemical reduction of CO₂ to formate at high current density using gas diffusion electrodes, *J. Appl. Electrochem.*, 44 (2014) 1107-1116.

- [46] H. Zhong, K. Fujii, Y. Nakano, Effect of KHCO_3 , K_2CO_3 and CO_2 on the Electrochemical Reduction of CO_2 into Organics on a Cu Electrode for the Solar Energy Conversion and Storage, *MRS Proceedings*, 1640 (2014) Mrsf13-1640-z1610-1652.
- [47] Gurudayal, J. Bullock, D.F. Srankó, C.M. Towle, Y. Lum, M. Hettick, M.C. Scott, A. Javey, J.W. Ager, Efficient solar-driven electrochemical CO_2 reduction to hydrocarbons and oxygenates, *Energy Environ. Sci.*, 10 (2017) 2222-2230.
- [48] S. Lee, S. Hong, J. Lee, Bulk pH contribution to CO/HCOO^- production from CO_2 on oxygen-evacuated Cu_2O electrocatalyst, *Catalysis Today*, 288 (2016) 11-17.
- [49] Y. Song, R. Peng, D.K. Hensley, P.V. Bonnesen, L. Liang, Z. Wu, H.M. Meyer, M. Chi, C. Ma, B.G. Sumpter, A.J. Rondinone, High-Selectivity Electrochemical Conversion of CO_2 to Ethanol using a Copper Nanoparticle/N-Doped Graphene Electrode, *ChemistrySelect*, 1 (2016) 6055-6061.
- [50] R. Kortlever, K.H. Tan, Y. Kwon, M.T.M. Koper, Electrochemical carbon dioxide and bicarbonate reduction on copper in weakly alkaline media, *J. Solid State Electrochem.*, 17 (2013) 1843-1849.
- [51] S.Y. Choi, S.K. Jeong, H.J. Kim, I.-H. Baek, K.T. Park, Electrochemical Reduction of Carbon Dioxide to Formate on Tin–Lead Alloys, *ACS Sustain. Chem. Eng.*, 4 (2016) 1311-1318.
- [52] Y. Chen, M.W. Kanan, Tin oxide dependence of the CO_2 reduction efficiency on tin electrodes and enhanced activity for tin/tin oxide thin-film catalysts, *J. Am. Chem. Soc.*, 134 (2012) 1986-1989.
- [53] P.G. Russell, N. Kovac, S. Srinivasan, M. Steinberg, The Electrochemical Reduction of Carbon Dioxide, Formic Acid, and Formaldehyde, *J. Electrochem. Soc.*, 124 (1977) 1329.
- [54] M. Schreier, L. Curvat, F. Giordano, L. Steier, A. Abate, S.M. Zakeeruddin, J. Luo, M.T. Mayer, M. Gratzel, Efficient photosynthesis of carbon monoxide from CO_2 using perovskite photovoltaics, *Nat. Commun.*, 6 (2015) 7326-7331.
- [55] S.R. Narayanan, B. Haines, J. Soler, T.I. Valdez, Electrochemical Conversion of Carbon Dioxide to Formate in Alkaline Polymer Electrolyte Membrane Cells, *J. Electrochem. Soc.*, 158 (2011) A167-A173.
- [56] Y. Hori, S. Suzuki, Cathodic Reduction of Carbon Dioxide for Energy Storage, *Journal of the Research Institute for Catalysis Hokkaido University*, 30 (1982) 81-88.
- [57] P.W. Atkins, J. de Paula, *Kurzlehrbuch Physikalische Chemie*, 4th ed., Wiley-VCH, , Weinheim, 2008.
- [58] Q. Zhang, H. Chen, T. Wu, T. Jin, Z. Pan, J. Zheng, Y. Gao, W. Zhuang, The opposite effects of sodium and potassium cations on water dynamics, *Chem. Sci.*, 8 (2017) 1429-1435.
- [59] K.E. Heusler, Multicomponent electrodes, *Electrochim. Acta*, 41 (1996) 411-418.
- [60] F. Zhang, J. Ding, Y. Zhang, M. Chen, Z.W. Ding, M.C. van Loosdrecht, R.J. Zeng, Fatty acids production from hydrogen and carbon dioxide by mixed culture in the membrane biofilm reactor, *Water Res.*, 47 (2013) 6122-6129.

- [61] L.T. Angenent, H. Richter, W. Buckel, C.M. Spirito, K.J.J. Steinbusch, C.M. Plugge, D.P.T.B. Strik, T.I.M. Grootscholten, C.J.N. Buisman, H.V.M. Hamelers, Chain Elongation with Reactor Microbiomes: Open-Culture Biotechnology To Produce Biochemicals, *Environ. Sci. Technol.*, 50 (2016) 2796-2810.
- [62] D. Ou, H. Li, W. Li, X. Wu, Y.Q. Wang, Y.D. Liu, Salt-tolerance aerobic granular sludge: Formation and microbial community characteristics, *Bioresour. Technol.*, 249 (2017) 132-138.
- [63] A. Sydow, T. Krieg, R. Ulber, D. Holtmann, Growth medium and electrolyte - how to combine the different requirements on the reaction solution in bioelectrochemical systems using *Cupriavidus necator*, *Eng. Life Sci.*, 17 (2017) 781-791.
- [64] J.M. Friedrich, C. Ponce-de-León, G.W. Reade, F.C. Walsh, Reticulated vitreous carbon as an electrode material, *J. Electroanal. Chem.*, 561 (2004) 203-217.
- [65] T. Warnecke, R.T. Gill, Organic acid toxicity, tolerance, and production in *Escherichia coli* biorefining applications, *Microb. Cell Fact.*, 4 (2005) 25-32.
- [66] C. Kirkpatrick, L.M. Maurer, N.E. Oyelakin, Y.N. Yoncheva, R. Maurer, J.L. Slonczewski, Acetate and formate stress: opposite responses in the proteome of *Escherichia coli*, *J. Bacteriol.*, 183 (2001) 6466-6477.